

Structure and dynamics of the negative thermal expansion material Cd(CN)₂ under pressure

Chloe S. Coates,^{1,2} Mia Baise,³ Johnathan M. Bulled,¹ Emma H. Wolpert,^{1,4} Joshua W. Makepeace,^{1,5} Helen C. Walker,⁶ Alexandra S. Gibbs,^{6,7} A. Dominic Fortes,⁶ Ben Slater,³ and Andrew L. Goodwin^{1,*}

¹*Department of Chemistry, University of Oxford, Inorganic Chemistry Laboratory, South Parks Road, Oxford OX1 3QR, U.K.*

²*Department of Chemistry, University of Cambridge, Lensfield Road, Cambridge CB2 1EW, U.K.*

³*Department of Chemistry, 20 Gordon Street, University College London, WC1H 0AJ, U.K.*

⁴*Department of Chemistry, Imperial College London, SW7 2AZ, U.K.*

⁵*School of Chemistry, University of Birmingham, Edgbaston, B15 2TT, U.K.*

⁶*ISIS Facility, Rutherford Appleton Laboratory, STFC, Didcot, OX11 0QX, U.K.*

⁷*School of Chemistry, University of St Andrews, North Haugh, St Andrews KY16 9ST, U.K.*

(Dated: February 21, 2023)

We use a combination of variable-temperature / variable-pressure neutron powder diffraction, variable-pressure inelastic neutron scattering, and quantum chemical calculations to interrogate the behaviour of the negative thermal expansion (NTE) material ¹¹⁴Cd(CN)₂ under hydrostatic pressure. We determine the equation of state of the ambient-pressure phase, and discover the so-called ‘warm hardening’ effect whereby the material becomes elastically stiffer as it is heated. We also identify a number of high-pressure phases, and map out the phase behaviour of Cd(CN)₂ over the range $0 \leq p \leq 0.5$ GPa, $100 \leq T \leq 300$ K. As expected for an NTE material, the low-energy phonon frequencies are found to soften under pressure, and we determine an effective Grüneisen parameter for these modes. Finally, we show that the elastic behaviour of Cd(CN)₂ is sensitive to the local Cd coordination environment, which suggests an interplay between short- (phononic) and long-timescale (cyanide flips) fluctuations in Cd(CN)₂.

I. INTRODUCTION

Negative thermal expansion (NTE) materials are useful and interesting because their structures contract—rather than expand—on heating [1–7]. Of the many different types of NTE systems now known, cadmium cyanide (Cd(CN)₂) is remarkable for a number of reasons. First, its NTE is isotropic: the Cd(CN)₂ structure has cubic symmetry [8–10], which is an attractive design consideration to minimise cracking in composites with tailored thermal expansion properties [1]. Second, the magnitude of its NTE effect is particularly large [9, 11]—indeed many times greater than that of well-known isotropic NTE materials such ZrW₂O₈ [12] and ScF₃ [13]. And, third, this NTE persists over an extremely large temperature window of about 600 K [11]. In fact its combination of NTE strength and persistence gives it the largest NTE capacity of all known materials [11, 14].

Mechanistically it has long been assumed that NTE arises in Cd(CN)₂ by the same processes operating in its better-studied congener Zn(CN)₂: namely, the thermal population of low-frequency phonons that act to draw the structure in on itself (so-called negative Grüneisen modes) [9, 15, 16]. But we have recently discovered that the cyanide ions in Cd(CN)₂ can in fact ‘flip’, and these long-timescale excitations act to enhance NTE further [17]. There turns out to be a surprising parallel between CN[−] flips in Cd(CN)₂ and spin-flips in the dipolar spin-ices such as Dy₂Ti₂O₇ [18–21]; this is a point to which we will return in due course.

Whatever the precise NTE mechanism may be, pressure is a particularly important thermodynamic variable for studying phonon-driven NTE systems [13, 22–26]. The Grüneisen pa-

rameter quantifies the effect of volume change on phonon frequencies, and the negative values associated with NTE modes imply that the corresponding mode frequencies are unstable under pressure [27]. Consequently, one expects to see displacive phase transitions in high-pressure studies of any phononic NTE material, with the distortions involved providing insight into the dominant NTE modes of the ambient phase [13, 23, 28]. It is common too for isotropic NTE materials to exhibit other counterintuitive mechanical phenomena at high pressure, such as amorphisation [22, 29–31] or pressure-induced softening—whereby a material becomes softer, rather than harder, as it is compressed [32].

Consequently, we sought to explore the structural and dynamical behaviour of Cd(CN)₂ as a function of hydrostatic pressure. Our approach is to use a combination of variable-pressure neutron scattering measurements (both elastic and inelastic) and quantum chemical calculations. An extreme sensitivity to damage by X-rays [11] rules out the use of variable-pressure X-ray diffraction measurements, and we highlight that our use of neutron scattering is feasible only because we have access to a ¹¹⁴Cd-enriched sample [17, 33]. Our key results are (i) the measurement of the equation of state of ambient-phase Cd(CN)₂, (ii) the discovery of strong pressure-induced softening and ‘warm hardening’ effects, (iii) explicit measurement of the pressure-induced phonon mode softening associated with negative Grüneisen modes, (iv) the identification of a series of high-pressure phases and their thermal stability, and (v) the identification of interplay between cadmium coordination environments and elastic moduli.

Our paper begins with a brief review of what is known regarding NTE in Cd(CN)₂, and also some of the key implications of the spin-ice model developed elsewhere to describe its physics. In Section III we provide details of the various methodologies used in our study—both experimental and computational. We then report our results, beginning with

*Electronic address: andrew.goodwin@chem.ox.ac.uk

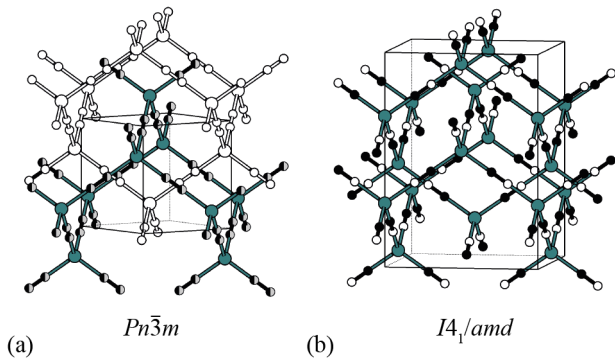


FIG. 1: (a) Representation of the cubic structure of ambient-phase $\text{Cd}(\text{CN})_2$ -I. Cd atoms are shown in teal, and C/N atoms (which are disordered) in dual-tone black/gray. One of the two interpenetrating diamondoid nets is coloured white. (b) The tetragonal $\text{Cd}(\text{CN})_2$ structure that emerges at ambient pressure for temperatures below about 135 K. C and N atoms are now shown in black and white, respectively; note the presence of cyanide-ion orientational order. The two frameworks have slipped relative to one another along the tetragonal (vertical) axis.

the effect of pressure at ambient temperature, and proceeding thereafter to consider the way in which this behaviour varies as temperature is reduced. The paper concludes with a discussion of the implications of our findings and a summary of the most important outstanding questions that remain to be addressed in future studies.

II. CADMIUM CYANIDE: BACKGROUND

At room temperature and ambient pressure, $\text{Cd}(\text{CN})_2$ adopts the anticuprite structure type with $Pn\bar{3}m$ crystal symmetry [Fig. 1(a)] [8–10, 17]. Cd centres are tetrahedrally coordinated by cyanide ions, and each cyanide ion bridges a pair of Cd^{2+} ions. These Cd–C–N–Cd linkages connect to form a network with the diamond topology; two such nets interpenetrate. The compounds $\text{Zn}(\text{CN})_2$ and $\text{Mn}(\text{CN})_2$ are isostructural to $\text{Cd}(\text{CN})_2$ [34–36]. All three systems show head-to-tail disorder of the cyanide ion orientations [17, 37, 38].

As is the case for $\text{Zn}(\text{CN})_2$ (and, presumably, $\text{Mn}(\text{CN})_2$), the cubic unit cell of $\text{Cd}(\text{CN})_2$ expands on cooling [9]. This NTE effect is quantified by the volumetric coefficient of thermal expansion, defined as the relative rate of change in volume at constant pressure:

$$\alpha_V = \frac{1}{V} \left(\frac{\partial V}{\partial T} \right)_p. \quad (1)$$

Variable-temperature powder X-ray diffraction measurements give the value $\alpha_V = -55(2) \text{MK}^{-1}$ for $\text{Cd}(\text{CN})_2$ at ambient pressure over the temperature range 150–750 K [11]. For context, the corresponding values for the high-profile isotropic NTE materials ScF_3 and ZrW_2O_8 are -12MK^{-1} (10–1100 K) and -26.1MK^{-1} (0.3–1050 K), respectively [12, 13].

Grüneisen theory provides a semi-quantitative rationalisation for NTE in $\text{Cd}(\text{CN})_2$ in terms of thermal population of volume-reducing phonon modes. For each branch of the phonon spectrum ν and for each wave-vector \mathbf{q} , the mode Grüneisen parameter

$$\gamma(\nu, \mathbf{q}) = - \frac{d[\ln \omega(\nu, \mathbf{q})]}{d(\ln V)} \quad (2)$$

is a dimensionless quantity that captures the coupling between phonon frequency ω and crystal volume V [3, 39]. Intuitively, one expects vibrational frequencies to increase with decreasing volume (shorter bonds = stiffer bonds), and hence $\gamma(\nu, \mathbf{q}) > 0$. NTE modes, by contrast, are vibrations for which $\gamma < 0$: like a plucked guitar-string, their frequency drops as the system is compressed. The bulk Grüneisen parameter $\gamma(T)$ integrates over all modes and all periodicities, with the contribution of each $\gamma(\nu, \mathbf{q})$ weighted by the corresponding contribution of the mode to the specific heat at temperature T . Hence $\gamma(T)$ is negative if and only if there is a large number of individual $\gamma(\nu, \mathbf{q}) < 0$ terms for modes with low frequencies. The explicit link to NTE comes *via* the relationship

$$\alpha_V = \frac{\gamma C_V}{VB}, \quad (3)$$

where B is the isothermal bulk modulus and C_V the specific heat at constant volume. Since V , B , and C_V are all strictly positive, phonon-mediated isotropic NTE implies a negative value of γ . For $\text{Cd}(\text{CN})_2$, the Grüneisen parameters calculated using *ab initio* density functional theory (DFT) methods adopt a range of values between -20 and 2 and collectively give $\alpha_V = -39 \text{MK}^{-1}$ [15, 16].

Ultimately the vibrational modes responsible for NTE—*i.e.* those with large and negative Grüneisen parameters—appear to involve transverse displacements of CN^- ions away from the Cd...Cd axes, as envisaged in Refs. 9, 40 and implicated in other ‘tension-effect’ NTE materials [2].

An important early indication that the physics of $\text{Cd}(\text{CN})_2$ might be more complicated than implied by this relatively conventional picture was the experimental observation of a displacive phase transition on cooling below 150 K that occurs despite the absence of any phonon instabilities identified in DFT calculations [9, 10, 15]. We have recently shown that this transition is driven by temperature-dependent ordering of CN^- ion orientations, and hence there is strong coupling between long-timescale CN^- ion ‘flips’ and the elastic behaviour of $\text{Cd}(\text{CN})_2$ [17]. The thermal accessibility of CN^- flips distinguishes the behaviour of $\text{Cd}(\text{CN})_2$ from that of its better-studied analogue $\text{Zn}(\text{CN})_2$. Cyanide orientations are fixed in the latter [38, 41] and its ambient-temperature $Pn\bar{3}m$ structure is stable down to the very lowest temperatures for which crystallographic data have been measured (25 K) [9].

The low-temperature structure of $\text{Cd}(\text{CN})_2$, as determined using neutron scattering measurements, has tetragonal $I4_1/amd$ symmetry [Fig. 1(b)] [17]. This structure differs from that of the ambient $Pn\bar{3}m$ phase in two key respects. First, the cyanide orientations are no longer disordered, but

are progressively arranged such that each Cd centre is coordinated by two C and two N atoms. This allows the Cd atom to displace away from the centre of the CdC_2N_2 coordination tetrahedron, giving rise to a local dipole [10, 17]. Within each of the two interpenetrating diamondoid nets these dipoles point along a single common direction (parallel to one of the $\langle 100 \rangle$ axes of the original cubic cell), but the dipole orientation inverts from one net to the other to give antiferroelectric cyanide order. The second key difference is that the two interpenetrating diamondoid networks—evenly spaced in the ambient $Pn\bar{3}m$ structure—are displaced in opposite directions along the tetragonal axis at low temperatures. The relationship between ambient- and low-temperature $\text{Cd}(\text{CN})_2$ structures is similar to that between the high-pressure VII and VIII phases of water ice [42–44].

In Ref. 17 we rationalised this particular CN^- ordering transition in terms of a simple pseudospin model of CN^- dipolar degrees of freedom. Denoting the orientation of each CN^- ion by a classical vector \mathbf{S} , we found that the ‘spin-ice’-like Hamiltonian

$$\mathcal{H} = -J_{\text{eff}} \sum_{i,j} \mathbf{S}_i \cdot \mathbf{S}_j + D \sum_{i,j'} \mathbf{S}_i \cdot \mathbf{S}_{j'} - \Delta \sum_i S_{i\parallel}^2 \quad (4)$$

actually captured the key physics of CN^- order and disorder in $\text{Cd}(\text{CN})_2$ surprisingly well. Here, J_{eff} , D , and Δ correspond respectively to an effective interaction between nearest-neighbour CN^- ions in the same network, an interaction between nearest-neighbour CN^- ions in alternate networks, and a ‘single-ion’ term that reflects the barrier height to CN^- flips. Experiment and theory converge on essentially the same set of values $J_{\text{eff}} = 205$ K, $D = 85$ K, $\Delta = 8\,800$ K, for which Eq. (4) predicts a phase transition at $T_c = 121$ K to precisely the $I4_1/amd$ structure type observed experimentally. Since the CN^- flipping mechanism involves a decrease in Cd...Cd separation, one expects some interplay between CN^- flips and NTE, and again between these flips and the behaviour of $\text{Cd}(\text{CN})_2$ under pressure.

Whereas the effect of pressure on the structural and spectroscopic behaviour of $\text{Zn}(\text{CN})_2$ has been relatively extensively studied [27, 28, 45–50], to the best of our knowledge the only variable-pressure investigation of $\text{Cd}(\text{CN})_2$ is the early infrared study of Ref. 45. That work identified a single phase transition at pressure < 3 GPa in which the Cd environment appeared to increase in symmetry. Any attempts to determine the structural evolution of $\text{Cd}(\text{CN})_2$ using variable-pressure X-ray diffraction measurements will have suffered from the extreme sensitivity to X-ray damage that severely complicates reliable structure determination [11].

III. METHODS

Here we investigate the high-pressure behaviour of $\text{Cd}(\text{CN})_2$ using a variety of experimental and computational approaches. In this section we provide details of the specific methods used in our study.

A. Synthesis

A sample of isotopically enriched $\text{Cd}(\text{CN})_2$ was prepared according to the method outlined in Ref. 33. $\text{Hg}(\text{CN})_2$ (1 g, Aldrich, 99%) and excess ^{114}Cd metal (1 g, Isoflex, 99.1(3)% ^{114}Cd) were added to one arm of a custom-made glass N-cell. Anhydrous ammonia gas (30 mL liquid ammonia volume, BOC) was condensed onto the mixture and stirred for six hours in an acetone/dry-ice bath with the temperature maintained between 240 and 250 K. The mixture was filtered—through the porous frit separating the two Schlenk tubes of the N-cell—under flowing ammonia gas to remove insoluble Hg. The resulting solution allowed to evaporate, yielding a polycrystalline sample of $^{114}\text{Cd}(\text{NH}_3)_2[^{114}\text{Cd}(\text{CN})_4]$. This was then heated at 80°C for 24 hours to yield $^{114}\text{Cd}(\text{CN})_2$. The sample used here is the same as that on which the earlier neutron scattering study of Ref. 17 was based.

B. Variable-temperature/variable-pressure neutron diffraction measurements

Variable-temperature/variable-pressure neutron diffraction measurements were carried out using the HRPD and OSIRIS instruments at the ISIS spallation source.

For the HRPD measurements, 1.3658 g of $^{114}\text{Cd}(\text{CN})_2$ was loaded into a TiZr gas pressure cell, which was then pressurised with argon gas as the pressure-transmitting medium. The hydrostatic pressure was generated by an external pressure intensifier unit to an accuracy of 1 bar. Ar was chosen instead of He to avoid penetration of the smaller He atoms inside the $\text{Cd}(\text{CN})_2$ framework structure. The temperature was controlled using a closed cycle refrigerator (CCR) between 300 and 100 K. Data were collected on increasing pressure between 0 and 0.5 GPa in 0.1 GPa increments. The initial pressure was 50 bar (0.005 GPa) to ensure that the pressure cell was sealed. At each pressure point data were collected on cooling at five temperatures (300, 250, 200, 150 and 100 K), after which the temperature was raised to 300 K and the pressure increased. Data collections of $80\ \mu\text{A}$ (~ 2 hours) were carried out at each point, using the instrument’s standard 30–130 ms time-of-flight window. Due to the substantial incoherent background produced by the TiZr alloy, which overwhelms the coherent scattering from the sample in backscattering geometry, only data from HRPD’s 90-degree detector banks were used for profile refinement. The time-of-flight bands stated above correspond to d -spacing ranges of 0.85–3.90 Å in the 90-degree detectors.

For the OSIRIS measurements, 1.300 g of $^{114}\text{Cd}(\text{CN})_2$ was loaded into a TAV-6 (Ti-6Al-4V alloy) gas pressure cell. Unlike the TiZr cell, TAV-6 is not null scattering, but contains well-defined Bragg peaks at low d -spacing and has a negligible incoherent background signal [51]. An additional advantage of this cell is that the greater strength of the TAV-6 alloy relative to TiZr allows the pressure vessel’s walls to be thinned from 10.5 to 5.3 mm, whilst still achieving a maximum working pressure of 0.54 GPa. This greatly reduces the attenuation of the incident beam and of the diffracted

rays. The cell was then pressurised using Ar gas as the pressure-transmitting medium up to a minimum starting pressure of 10 bar (0.001 GPa). Data were collected using two separate time-of-flight bands in order to access an appropriate d -spacing range in the instrument's only available diffraction detectors, which are positioned in backscattering geometry. The corresponding time-of-flight bandwidths were 29.4–69.4 ms and 47.1–87.1 ms, giving d -ranges of 1.8–4.0 Å and 2.9–4.9 Å, respectively. The experimental protocol was chosen in order to maximise the number of data points within the ambient $Pn\bar{3}m$ phase. Data were collected in intervals of 0.02 GPa from 0–0.2 GPa at 300 K, before cooling to 275 K (at pressure). The gas cell was then depressurised after a period of two hours (the time deemed necessary for the induced activity of Ar to decay to a level at which the gas could be safely vented). Once at 275 K, data were again collected in intervals of 0.02 GPa up to 0.2 GPa before cooling to 250 K at pressure, and then depressurising to 0.005 GPa. Again, data were measured in 0.02 GPa increments up to 0.18 GPa at 250 K, at which point there appeared to be evidence of sample history dependence. The sample was then warmed to 300 K at 0.2 GPa before depressurising at 300 K, then cooling to 250 K, at which point the pressure points 0–0.2 GPa were repeated in 0.02 GPa increments.

Pawley refinements were carried out using TOPAS Academic v.4.1 [52] to obtain the T/p dependence of the cubic lattice parameter of $\text{Cd}(\text{CN})_2$. The instrument-dependent peak shape parameters were refined against diffraction data for a Si 640c NIST standard. The Bragg peaks corresponding to the TAV-6 pressure cell were refined as two Pawley phases, the first corresponding to the structure of hcp-Ti with space group symmetry $P6_3/mmc$ ($a \sim 2.924$ Å, $c \sim 4.670$ Å) and a second fcc phase with $Fm\bar{3}m$ symmetry ($a \sim 4.532$ Å). Lattice parameters used in the equation of state for $\text{Cd}(\text{CN})_2$ were obtained using Pawley refinements. For the OSIRIS data, the d -range used for Pawley refinements was confined to $3 < d < 4.6$ Å. Three peaks corresponding to the (002), (111) and (011) $Pn\bar{3}m$ Bragg reflections were measured in this region at all pressures. The signal at lower d -spacings was dominated by strong reflections from the TAV-6 sample container, and so this region was not used for Pawley refinements for lattice parameter determination.

C. Variable-pressure inelastic neutron scattering measurements

Variable-pressure inelastic neutron scattering experiments were performed at ambient temperature on the same ~ 1 g of $^{114}\text{Cd}(\text{CN})_2$ described above using the MARI instrument at ISIS. The incident neutron energy was 10 meV (400 Hz choppers), which gave an energy resolution of about 0.175 meV at an energy transfer of 2 meV. Pressure was applied using a recently developed low-background, cylindrical clamp cell made of TAV-6, an alloy which minimises unwanted absorption and background scattering that often complicate high-pressure inelastic neutron scattering experiments using He as pressure-transmitting medium. Each measurement

corresponded to a neutron beam exposure of approximately 1000 $\mu\text{A h}$ and was corrected for background scattering from the sample environment.

D. Quantum mechanical calculations

Ab initio lattice dynamical calculations were performed using the PAW formalism [53] as implemented in VASP [54–56]. We used PBE functionals with a plane-wave cut-off of 1600 eV to avoid Pulay stress [57, 58]. Electronic self-consistent field cycles were converged to 10^{-6} eV and the convergence criteria for the total energy and ionic forces were set to 10^{-8} eV and 10^{-6} eV Å $^{-1}$, respectively. The structures were allowed to fully relax—ions and lattice parameters were optimised simultaneously—for different representative $\text{Cd}(\text{CN})_2$ models to account for varying degrees of cyanide order. These relaxed cells were then used as the basis for elastic property calculations. In each case, we generated a series of seven structures with expanded/contracted cells $-0.5 < \Delta V/V < +0.5\%$. The volume dependence of the energy was fitted using a third-order Birch-Murnaghan equation of state in order to determine the zero-pressure bulk modulus B_0 and its first pressure derivative B'_0 [59]. Phonon dispersion relations were calculated using the PHONOPY package [60], and thermal expansivities determined within the quasi-harmonic approximation using PHONOPY-qha [61].

IV. RESULTS AND DISCUSSION

A. $\text{Cd}(\text{CN})_2$ -I equation of state

Our starting point was to explore the structural behaviour of $\text{Cd}(\text{CN})_2$ under compression at ambient temperature. Fig. 2(a) shows the evolution of a key region of the neutron diffraction pattern as a function of pressure, as measured using the OSIRIS instrument. From these data, it is clear that the ambient-pressure phase is stable only up to a pressure of about 0.14 GPa whereupon it undergoes a first-order transition to a high-pressure phase. We hereafter use the labels $\text{Cd}(\text{CN})_2$ -I and $\text{Cd}(\text{CN})_2$ -II to denote the ambient and high-pressure phases. Pawley refinements against the neutron diffraction patterns measured at varying pressure values allowed extraction of the $V(p)$ equation of state, which is shown in Fig. 2(b). We used the third-order Birch Murnaghan formalism [62, 63]

$$p(V) = \frac{3B_0}{2} \left[\left(\frac{V_0}{V} \right)^{\frac{7}{3}} - \left(\frac{V_0}{V} \right)^{\frac{5}{3}} \right] \times \left\{ 1 + \frac{3}{4}(B'_0 - 4) \left[\left(\frac{V_0}{V} \right)^{\frac{2}{3}} - 1 \right] \right\} \quad (5)$$

to fit these data and so estimate the zero-pressure bulk modulus B_0 and its pressure dependence B'_0 . In this way, we obtained $B_0 = 13.6(4)$ GPa and $B'_0 = -18(5)$. The corresponding value of V_0 was 251.271(19) Å 3 .

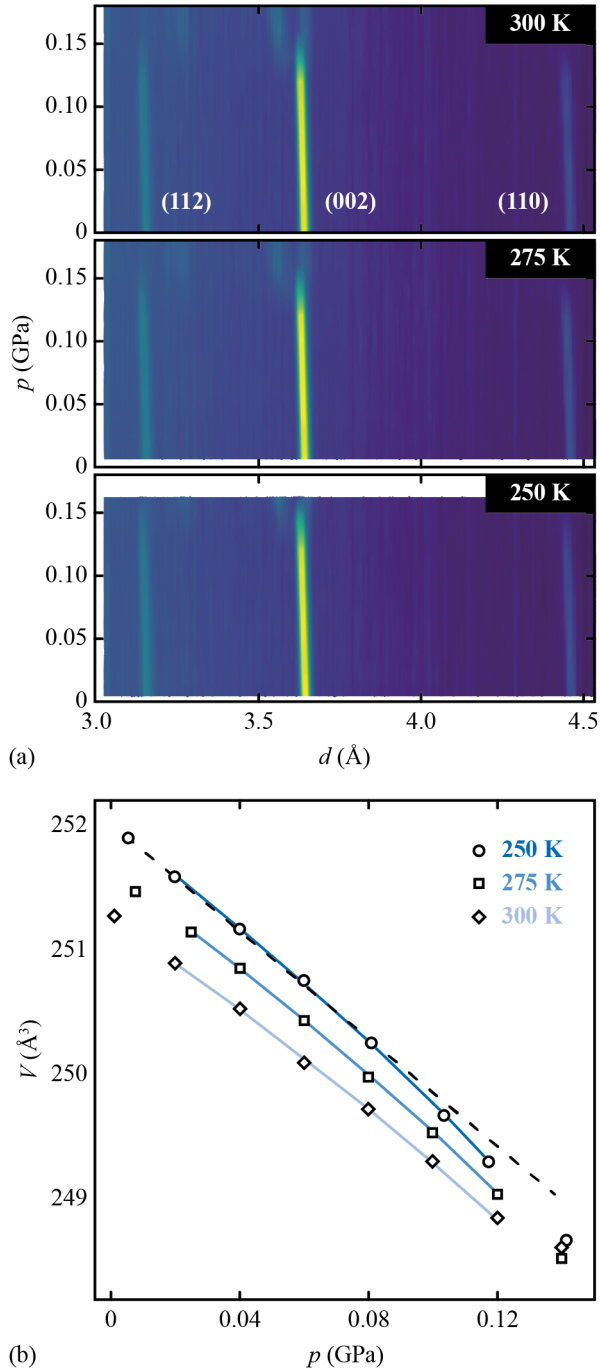


FIG. 2: (a) Variable-pressure neutron diffraction patterns of $\text{Cd}(\text{CN})_2\text{-I}$ at 300, 275 and 250 K. At each temperature there is a first-order transition to a lower-symmetry phase at a critical pressure of about 0.14 GPa. (b) Equation of state of $\text{Cd}(\text{CN})_2\text{-I}$, with data extracted *via* Pawley refinement against the diffraction patterns shown in (a). The solid curves correspond to fits obtained using Eq. (6); in these fits we have excluded the lowest- and highest-pressure data points as a consequence of the increased experimental uncertainty at these extremes. The dashed line shows a linear fit to the 250 K data, so as to emphasise the extreme pressure-induced softening observed at this temperature.

We put these values in context by contrasting the pressure-dependent behaviour of $\text{Cd}(\text{CN})_2$ with that of its better-studied close relative $\text{Zn}(\text{CN})_2$. There are a few key differences. First, the former is about three times softer than the latter ($B_0 = 36.9(22)$ GPa in $\text{Zn}(\text{CN})_2$) [28, 46]. While both materials become softer as pressure is increased—the anomalous ‘pressure-induced softening’ effect characteristic of NTE materials [32, 50]— $\text{Cd}(\text{CN})_2$ does so about three times as quickly as $\text{Zn}(\text{CN})_2$ (for which $B'_0 = -6.0(7)$) [28, 46]. So $\text{Cd}(\text{CN})_2$ is elastically very soft, and becomes even softer very quickly under pressure. This description is consistent with our observation of a pressure-induced phase transition at remarkably low pressures: indeed $\text{Cd}(\text{CN})_2\text{-I}$ is about an order of magnitude less stable to compression than $\text{Zn}(\text{CN})_2\text{-I}$, which persists to ~ 1.5 GPa [28].

Since the $\text{Cd}(\text{CN})_2\text{-I}$ structure is known to be stable at ambient pressure on cooling to ~ 150 K, we repeated our isothermal high-pressure neutron diffraction measurements at reduced temperatures of 275 and 250 K. The corresponding data are shown in Fig. 2(a). We observed qualitatively similar behaviour at both temperatures to that observed at 300 K—in that the ambient phase is stable only up to pressures of about 0.14 GPa. The critical pressure appeared to show very little temperature dependence, and we noted from diffraction measurements performed on decompression (data not shown) a hysteresis in the $\text{Cd}(\text{CN})_2\text{-I/II}$ transition. The corresponding unit-cell volumes were again extracted from our variable-pressure diffraction patterns using Pawley refinements, and we show the corresponding data in Fig. 2(b). As expected for an NTE material, the unit-cell volume increases on cooling. Also evident is an increased pressure-induced softening effect as temperature is reduced.

To quantify the combination of both thermal and pressure effects, we used a modified version of the third-order Birch-Murnaghan expression

$$p(V, T) = \frac{3B_0(T)}{2} \left[\left(\frac{V_0(T)}{V} \right)^{\frac{7}{3}} - \left(\frac{V_0(T)}{V} \right)^{\frac{5}{3}} \right] \times \left\{ 1 + \frac{3}{4}(B'_0 - 4) \left[\left(\frac{V_0(T)}{V} \right)^{\frac{2}{3}} - 1 \right] \right\}, \quad (6)$$

where

$$V_0(T) = V_0(T_{\text{ref}})[1 + \alpha_V(T - T_{\text{ref}})] \quad (7)$$

and

$$B_0(T) = B_0(T_{\text{ref}}) + \left(\frac{\partial B}{\partial T} \right)_p (T - T_{\text{ref}}). \quad (8)$$

Here we have included the lowest-order terms that allow for variation in system volume and stiffness as a function of temperature. We used the intermediate temperature value (275 K) as T_{ref} , and fitted Eq. (6) to the ensemble of variable- p/T unit-cell data measured at 250, 275, and 300 K. The corresponding fits give $B_0(T_{\text{ref}}) = 13.5(2)$ GPa, $B'_0 = -26(3)$, $\alpha_V = -60.0(13)$ MK^{-1} , and $(\frac{\partial B}{\partial T})_p = 0.030(3)$ GPa K^{-1} .

The last of these parameters, which quantifies the thermal variation in material stiffness, deserves particular comment.

That the value obtained is positive for $\text{Cd}(\text{CN})_2$ implies that the bulk modulus increases with temperature. This effect—termed *warm hardening*—is counterintuitive because materials normally soften on heating [7]. Its origin in NTE materials is thought to involve an increased anharmonicity of NTE modes at higher temperatures [7, 26]. Thermodynamically, the quantity is related to the isothermal pressure dependence of the expansivity: [7]

$$\left(\frac{\partial\alpha_V}{\partial p}\right)_T = \frac{1}{B^2} \left(\frac{\partial B}{\partial T}\right)_p. \quad (9)$$

So, we find that the magnitude of NTE in $\text{Cd}(\text{CN})_2$ is actually reduced under pressure—*i.e.* $(\frac{\partial\alpha_V}{\partial p})_T > 0$. This observation again runs counter to intuition: one might reasonably expect that, since NTE modes decrease in energy with applied pressure, NTE should be *enhanced* as pressure is increased. $\text{Zn}(\text{CN})_2$ is conventional in this respect, as its room-temperature NTE effect increases in magnitude from ambient pressure ($\alpha_V = -52.2(5) \text{ MK}^{-1}$) to 0.4 GPa ($\alpha_V = -58.2(6) \text{ MK}^{-1}$) [46]. The anomalous behaviour of $\text{Cd}(\text{CN})_2$ again reflects the argument made in Refs. 7, 26 that anharmonic effects—if sufficiently strong—can invert this relationship.

B. Inelastic neutron scattering

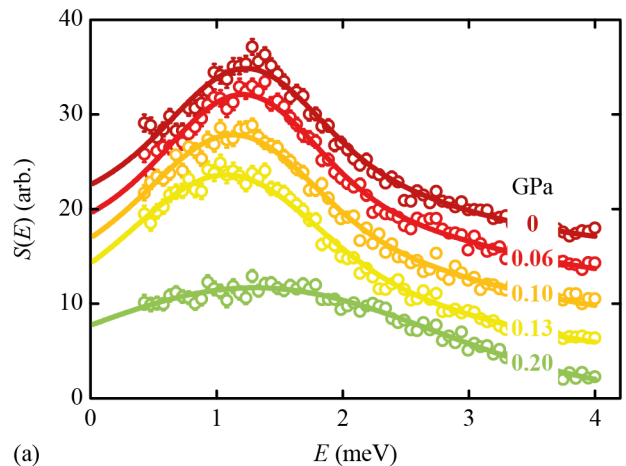
In order to provide further insight into anharmonicity in $\text{Cd}(\text{CN})_2$ -I, we used inelastic neutron scattering measurements to monitor the effect of pressure on the neutron-weighted phonon density of states. We carried out measurements at five pressure values: 0, 0.06, 0.1, 0.13, and 0.2 GPa. The Q -integrated $S(E) = \int S(Q, E) dQ$ inelastic neutron scattering function is shown in Fig. 3(a) for the low-energy domain $0 \leq E \leq 4 \text{ meV}$. This energy range includes the relatively dispersionless phonon branches understood to dominate NTE response [15]. Indeed, at all pressures, $S(E)$ is dominated by a single feature centred at $E \simeq 1.2 \text{ meV}$. For pressures below $p_c \simeq 0.14 \text{ GPa}$, the $S(E)$ function is very similar, with the position of the main feature shifting to lower energy as pressure increases. By contrast, the $S(E)$ function measured for $\text{Cd}(\text{CN})_2$ -II at 0.2 GPa is very different: while there is still a single peak, it is much broader and centred at a higher E .

We have quantified these various observations by fitting the $S(E)$ functions using a double Gaussian

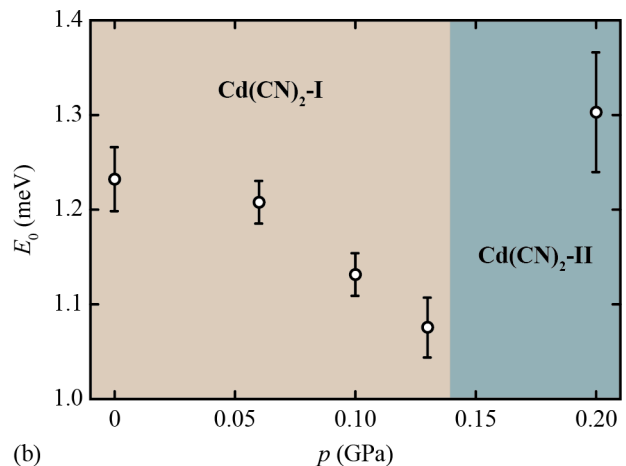
$$S(E) \simeq c_1 \exp\left[-\frac{(E - E_0)^2}{w_1^2}\right] + c_2 \exp\left[-\frac{(E - E_0)^2}{w_2^2}\right], \quad (10)$$

where the amplitudes c_i , widths w_i and position E_0 were treated as free parameters. We show in Fig. 3(b) the pressure-dependence of the peak position E_0 , which reflects the various observations noted above. Interpreting the value of E_0 as an approximation to the mean energy of the low-frequency phonon branches in $\text{Cd}(\text{CN})_2$ -I, we use the relation

$$\gamma = \frac{B_0}{E} \frac{dE}{dp}, \quad (11)$$



(a)



(b)

FIG. 3: (a) Neutron-weighted low-energy phonon densities of states in $\text{Cd}(\text{CN})_2$ measured using the MARI spectrometer. Data are shown as open circles, and fits using Eq. (10) are shown as solid lines. Successive curves have been shifted vertically by four units to aid interpretation. (b) Pressure dependence of the effective mean value E_0 of the low-energy phonon dispersion, obtained from the fits to data shown in (a). The decrease in E_0 with pressure is characteristic of NTE materials, for which γ is negative. The NTE modes appear to stiffen on progression into the high-pressure phase $\text{Cd}(\text{CN})_2$ -II.

derived from Eq. (2), to obtain the estimate $\gamma \simeq -14(3)$. Such a large and negative Grüneisen parameter (*cf.* $\gamma \simeq -1$ for ZrW_2O_8 , Ref. 64) is similar to the value $\gamma = -20$ determined for the lowest-energy NTE modes using density functional theory calculations [15].

C. Exploration of the wider p/T phase diagram

Variable-temperature / variable-pressure neutron diffraction measurements (HRPD instrument) were used to map the phase behaviour of $\text{Cd}(\text{CN})_2$ over a larger temperature and pressure domain. A total of 30 different p, T values were interrogated, spanning the ranges $0.005 \leq p \leq 0.5 \text{ GPa}$ and $100 \leq T \leq 300 \text{ K}$ [Fig. 4]. These p, T values were evenly spaced, and we note that the minimum pressure 0.005 GPa

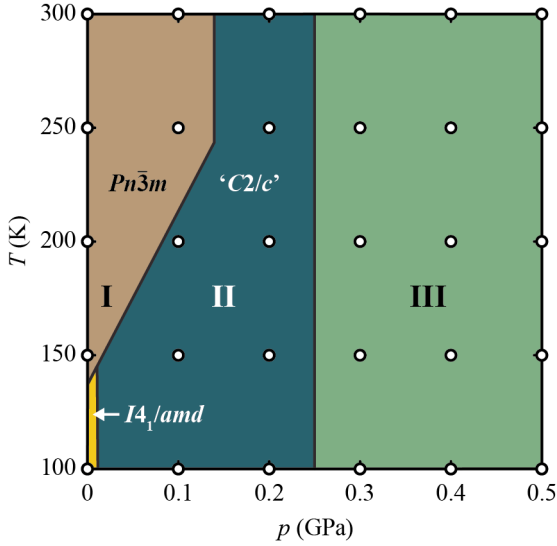


FIG. 4: Pressure/temperature phase diagram of $\text{Cd}(\text{CN})_2$ as determined using neutron diffraction measurements. The grid of (p, T) values interrogated using HRPD are shown as open white circles. This diagram includes the low-temperature ambient-pressure $I4_1/amd$ phase reported in Ref. 17.

corresponds to that required to seal the gas cell used in our measurements. In total we identified three distinct phases distributed across the p, T values we sampled, giving rise to the phase diagram shown in Fig. 4.

One surprise in this study was the observation of a different low-temperature phase transition at $p = 0.005$ GPa, $T \sim 120$ K to that reported using ambient-pressure neutron diffraction measurements in Ref. 17. We contrast in Fig. 5(a,b) the neutron diffraction patterns measured at a pressure of 0.005 GPa at 300 and 100 K. The former can be fit using the conventional $Pn\bar{3}m$ structure model but the latter is noticeably different from the $I4_1/amd$ neutron diffraction pattern reported in Ref. 17. Instead we found that the low-temperature 0.005 GPa phase gave a similar diffraction pattern to the high-pressure $\text{Cd}(\text{CN})_2$ -II phase studied at room temperature (using both HRPD and OSIRIS instruments) [Fig. 5(c)]. Hence the $\text{Cd}(\text{CN})_2$ -II structure appears to be favoured at both modest pressures and low temperatures, but clearly requires some small pressure to be stabilised relative to the $I4_1/amd$ ambient-pressure/low-temperature phase.

Our data were not of sufficient quality to allow structure solution of the $\text{Cd}(\text{CN})_2$ -II phase. We obtained a reasonable (but by no means perfect) match to the 100 K / 0.005 GPa HRPD diffraction pattern using a highly constrained Rietveld refinement. Our approach was as follows. Noting the splitting of the (202) and (220) reflections ($d \sim 3.6, 3.2 \text{ \AA}$, respectively) was consistent with symmetry-lowering of the $I4_1/amd$ cell to a monoclinic structure, we carried out a search of appropriate monoclinic subgroups. Using ISODISTORT [65], we found that activation of the Γ_4^+ and Γ_5^+ strain modes gave a $C2/c$ solution with appropriate peak splitting. The relationship between this $C2/c$ cell and its $I4_1/amd$ parent was as

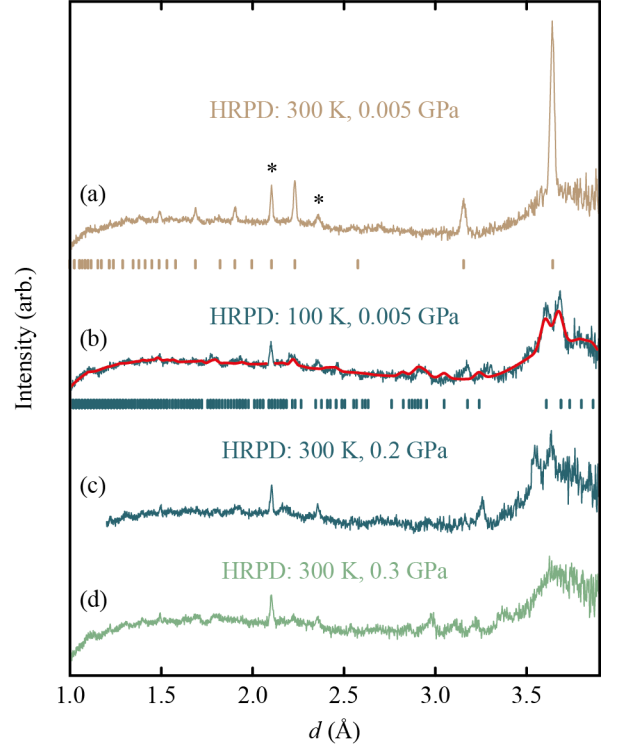


FIG. 5: Neutron diffraction patterns of $\text{Cd}(\text{CN})_2$ at specific key p, T values. (a) Ambient-phase $\text{Cd}(\text{CN})_2$ -I, indexed according to its $Pn\bar{3}m$ space-group symmetry. The two reflections marked by an asterisk are the strongest impurity peaks attributed to a small remnant $\text{Hg}(\text{CN})_2$ contaminant and are present in all patterns. (b) The low-temperature diffraction pattern obtained under minimum applied pressure. The tick marks denote expected reflection conditions for the $C2/c$ structure discussed in the text, and the red line shows the fit obtained using constrained Rietveld refinement. (c) Ambient-temperature diffraction pattern of $\text{Cd}(\text{CN})_2$ -II at $p = 0.2$ GPa. The general similarity between this pattern and that in (b) links the low-temperature and mid-pressure regimes in the phase diagram shown in Fig. 4. (d) Ambient-temperature diffraction pattern of $\text{Cd}(\text{CN})_2$ -III at $p = 0.3$ GPa.

follows:

$$\begin{bmatrix} \mathbf{a} \\ \mathbf{b} \\ \mathbf{c} \end{bmatrix}_{C2/c} = \begin{bmatrix} 0 & 0 & -1 \\ -1 & -1 & 0 \\ -\frac{1}{2} & \frac{1}{2} & \frac{1}{2} \end{bmatrix} \begin{bmatrix} \mathbf{a} \\ \mathbf{b} \\ \mathbf{c} \end{bmatrix}_{I4_1/amd}. \quad (12)$$

We then carried out a constrained Rietveld refinement in which the amplitudes of the Γ_4^+ and Γ_5^+ strain modes were allowed to vary, together with an overall scale factor and the conventional strain broadening terms. The background was fixed to that refined against the 150 K data set (*i.e.* when $\text{Cd}(\text{CN})_2$ is in its ambient-pressure $Pn\bar{3}m$ structure). Atom coordinates and atomic displacement parameters were constrained to those determined in the 100 K $I4_1/amd$ refinement of Ref. 17. The resulting fit is shown in Fig. 5(b). Taking into account the deficiencies of this fit, and the (understandably) reduced signal-to-noise of low-temperature high-pressure measurements, our assignment of $C2/c$ as the crystal symmetry of $\text{Cd}(\text{CN})_2$ -II is only tentative.

Whatever the true structure of $\text{Cd}(\text{CN})_2$ -II might be, the slope of the I/II phase boundary is nonetheless consistent with the positive value of $(\frac{\partial B}{\partial T})_p$ determined above for $\text{Cd}(\text{CN})_2$ -I. Our measured value of $0.030(3) \text{ GPa K}^{-1}$ implies a reduction of the bulk modulus of $\text{Cd}(\text{CN})_2$ -II by about 6 GPa on cooling from 300 to 100 K.

For all temperatures studied, we observed a further phase transition to another high-pressure phase at pressures $p_{c2} \simeq 0.25 \text{ GPa}$. This higher-pressure phase, which we denote $\text{Cd}(\text{CN})_2$ -III, gave a broad diffraction profile that we were unable to index with any confidence [Fig. 5(d)].

D. DFT calculations

Quantum chemical calculations were carried out to investigate the effect of ice-like cyanide ordering on the elastic properties of $\text{Cd}(\text{CN})_2$. Previous such calculations have been performed using the same high-symmetry cyanide-ordered structure ($P43m$) in which each Cd is coordinated by either four C atoms or four N atoms [15, 16]. The bulk modulus determined in this way was either 33.03 or 41.8 GPa, depending on whether GGA and LDA functionals were employed [16].

Our understanding of ambient-temperature $\text{Cd}(\text{CN})_2$ -I is that, despite the presence of cyanide orientational disorder, Cd coordination environments are nonetheless dominated by the CdC_2N_2 configuration, and so we interrogated the elastic properties of different ordered $\text{Cd}(\text{CN})_2$ arrangements with this local arrangement. The key results of our calculations are given in Table I. All four of the CdC_2N_2 states we studied gave bulk moduli smaller than that of the $P43m$ structure, even if they remained a little larger than the experimental value of 13.6 GPa. The key result here is that the adoption of ice-like coordination environments results in mechanical softening of the $\text{Cd}(\text{CN})_2$ structure. This observation is consistent with the warm-hardening effect noted experimentally (albeit *via* a mechanism distinct from that proposed in Ref. 7): as temperature increases, the relative fraction of ice-rule violations also increases, which (by our calculations) should result in a larger bulk modulus.

We also include in Table I the coefficients of thermal expansion determined using a quasiharmonic approach; in the same way that DFT overestimates B , it therefore also underestimates the magnitude of α_V . We expect that the discrepancy between experiment and calculation reflects the importance of anharmonicity in $\text{Cd}(\text{CN})_2$, and that finite-temperature simulations (*e.g.* molecular dynamics, MD) should provide better agreement between the two. This same effect was noted for $\text{Zn}(\text{CN})_2$, where a \sim twofold difference in B_0 values was found between 0 K DFT calculations and finite-temperature MD simulations governed by interatomic potentials fitted against those same calculations [26].

E. Role of spin-ice physics

We turn now to couch the pressure-dependent behaviour explicitly in terms of the spin-ice-like Hamiltonian of Equation 4

TABLE I: Bulk modulus and thermal expansion data for various $\text{Cd}(\text{CN})_2$ configurations obtained *via* lattice dynamical calculations.

Configuration	B_0 (GPa)	B'	α_V (MK^{-1})
CdC_2N_2 (1)	22.2	-34	-49
CdC_2N_2 (2)	24.4	-31	-46
CdC_2N_2 (3)	26.1	-29	-44
CdC_2N_2 (4)	31.6	-21	-34
$\text{CdC}_4/\text{CdN}_4$	33.2	-20	-31

developed in Ref. 17. In that particular study, we treated the electrostatic dipoles of CN^- ion as direct analogues of the magnetic dipoles in dipolar spin-ices [66]. QC calculations were used to derive the key interaction parameters J , D and Δ , from which the resulting thermal phase behaviour was determined. The key feature of the Hamiltonian, parameterised in this way, is that it exhibits a thermal phase transition between the low-temperature $I4_1/amd$ and $Pn\bar{3}m$ phases.

Our particular interest in the context of the variable-pressure behaviour of $\text{Cd}(\text{CN})_2$ is the parameter Δ , which quantifies the energy barrier to cyanide reorientation. It is obtained from nudged elastic band calculations, which also provide quantum-chemical evidence for the rotovibrational coupling observed in the correspondence between cyanide ordering and the evolution of the spontaneous strain [17]. The Cd...Cd distance is reduced during cyanide reorientation and couples to the unit-cell parameter in a simple geometric manner:

$$a = \frac{2}{\sqrt{3}} \left[d^\dagger + \langle S_{\parallel}^2 \rangle^{\frac{1}{2}} (d_0 - d^\dagger) \right]. \quad (13)$$

Here, S_{\parallel} is the projection of the cyanide ion pseudovector onto the corresponding Cd...Cd axis, which equals 0 at the mid-point of a cyanide-ion flip and 1 when the Cd-C-N-Cd linkage is perfectly linear. The values d_0 and d^\dagger correspond to the Cd...Cd distances for linear and mid-flip cyanide-ion geometries, respectively. Because cyanide-ion flips act to reduce a , they might be expected to occur increasingly often under the application of pressure.

We can estimate the contribution of cyanide reorientation to the elastic properties explicitly, starting from the thermodynamic relationship between the bulk modulus and the free energy $\phi(V)$ [7]:

$$B = V \frac{\partial^2 \phi}{\partial^2 V}. \quad (14)$$

In our model, the free energy associated with cyanide reorientation is $\phi(V) = 4\Delta \langle S_{\parallel}^2 \rangle$, where the factor of 4 reflects the number of cyanide pseudospins per $\text{Cd}(\text{CN})_2$ unit-cell. The expected volume can be extracted from the Cd...Cd distance, according to Equation (13), resulting in a final expression for the bulk modulus:

$$B = \frac{4\Delta}{(d_0 - d^\dagger)^2} \left(\frac{-1}{6a} + \frac{2d^\dagger}{3\sqrt{3}a^2} \right). \quad (15)$$

Using $\Delta = 8800\text{ K}$, [17] this expression gives $B = 24\text{ GPa}$ for $\text{Cd}(\text{CN})_2$, which is consistent with the value obtained directly from the quantum chemical calculations against which the spin-ice parameters were fitted. Hence the spin-ice description of $\text{Cd}(\text{CN})_2$ not only describes its thermal behaviour, but it also does a reasonable job of capturing the elastic behaviour of $\text{Cd}(\text{CN})_2$ -I. As a final point, we note that the relationship given by Eq. (15) captures within it the warm-hardening effect observed experimentally. As $\text{Cd}(\text{CN})_2$ -I is heated, a reduces (*i.e.* NTE), which in turn increases B .

V. CONCLUDING REMARKS

In this paper we have characterised the low-temperature/low-pressure phase behaviour of cadmium cyanide. $\text{Cd}(\text{CN})_2$ clearly exhibits pressure-dependent behaviour that is typical of an NTE material, in that it undergoes two symmetry lowering phase transitions at modest pressures ($< 0.3\text{ GPa}$) and displays pressure-induced softening. The particularly extreme softening, $B'_0 = -26(3)$, is a hallmark of an incipient elastic instability. The bulk modulus $B_0 = 13.5(2)\text{ GPa}$ is especially low—even amongst other flexible framework materials. The metal-organic framework UiO-66, for example, shows very large NTE with $\alpha_V = -70.2\text{ MK}^{-1}$ and has a bulk modulus of 26.5 GPa [67, 68]. We find that $\text{Cd}(\text{CN})_2$ is substantially softer than $\text{Zn}(\text{CN})_2$, and the lower pressures of the observed phase transitions reflect the intrinsic elastic instability of this system.

Whereas the thermodynamic behaviour of $\text{Zn}(\text{CN})_2$ was shown to be essentially insensitive to cyanide order [26], a key result here is that $\text{Cd}(\text{CN})_2$ models with different cyanide-ion orientations give rise to substantially different elastic properties. This finding suggests a strong coupling between cyanide-ion orientations and dynamic phenomena, that is reminiscent of rotovibrational coupling observed in alkali cyanides [69]. Potassium cyanide, for example, shows a rich phase behaviour as a function of temperature and pressure owing to competing quadrupolar and dipolar interactions between cyanide ions, with at least seven phases between $0 < T < 400\text{ K}$ and $0 < p < 3\text{ GPa}$ [70–74]. A particular challenge in understanding the physics of $\text{Cd}(\text{CN})_2$ then lies in the interplay of excitations occurring at vastly different timescales—*i.e.* the

cyanide-ion flips and phonon-driven fluctuations. This is a point to which we hope to return in future studies.

Here we have intentionally used gas cells to apply hydrostatic pressure to $\text{Cd}(\text{CN})_2$. Our motivation in doing so was to avoid the potential complication of interaction between the pressure-transmitting medium (PTM) and $\text{Cd}(\text{CN})_2$. In the case of $\text{Zn}(\text{CN})_2$, a large number of different high-pressure transformations occur as the PTM is varied [49]. One expects even more complex behaviour in the case of $\text{Cd}(\text{CN})_2$, since the Cd–C/N interactions are weaker than Zn–C/N, the $\text{Cd}(\text{CN})_2$ structure is larger and hence more open, and there is a remarkable empirical propensity for $\text{Cd}(\text{CN})_2$ to form clathrate structures [75–81]. Indeed, we cannot rule out the possibility that $\text{Cd}(\text{CN})_2$ -III phase involves structural reorganisation to include argon. The close relationship between the (presumed) $C2/c$ $\text{Cd}(\text{CN})_2$ -II structure and the low-temperature $I4_1/amd$ phase suggests that no chemical change has taken place at the I/II transition. A limitation of the use of gas-cell pressure chambers is that we have accessed only a relatively modest pressure range (albeit covering surprisingly rich structural behaviour). Future studies at higher pressures will likely reveal further phase transitions; in particular we anticipate the value of structural studies of the high-pressure phase transitions studied spectroscopically in Ref. 45.

Acknowledgments

The authors gratefully acknowledge financial support from the E.R.C. (Advanced Grant 788144 to A.L.G.) and the Leverhulme Trust (Grants RPG-2015-292 and RPG-2018-268). A.L.G. thanks Hanna Boström (Stuttgart), Nicholas Funnell (ISIS), Elinor Spencer (Virginia Tech), Nancy Ross (Virginia Tech), Andrew Cairns (Imperial), Andrew Seel (UCL) and Arkadiy Simonov (ETH Zurich) for useful discussions. We thank ISIS for the provision of neutron beamtime and the ISIS Pressure Group for technical assistance. The relevant experiment numbers and data locations are as follows. HRPD: RB1720214 (doi:10.5286/ISIS.E.89472889). OSIRIS: RB1820009 (doi:10.5286/ISIS.E.99689788). MARI: RB1920076 (doi:10.5286/ISIS.E.RB1920076) and RB2010632 (doi:10.5286/ISIS.E.RB2010632).

-
- [1] A. W. Sleight, *Ann. Rev. Mater. Sci.* **28**, 29 (1998).
 - [2] J. S. O. Evans, *J. Chem. Soc., Dalton Trans.* **19**, 3317 (1999).
 - [3] G. D. Barrera, J. A. O. Bruno, T. H. K. Barron, and N. L. Allan, *J. Phys.: Condens. Matter* **17**, R217 (2005).
 - [4] K. Takenaka, *Sci. Tech. Adv. Mater.* **13**, 013001 (2012).
 - [5] C. Lind, *Materials* **5**, 1125 (2012).
 - [6] C. J., L. Hu, J. X. Deng, and X. R. Xing, *Chem. Soc. Rev.* **44**, 3522 (2015).
 - [7] M. T. Dove and H. Fang, *Rep. Prog. Phys.* **79**, 066503 (2016).
 - [8] E. Shugam and H. Zhdanov, *Acta Physiochim. URSS* **20**, 247 (1945).
 - [9] A. L. Goodwin and C. J. Kepert, *Phys. Rev. B* **71**, 140301(R) (2005).
 - [10] V. E. Fairbank, A. L. Thompson, R. I. Cooper, and A. L. Goodwin, *Phys. Rev. B* **86**, 104113 (2012).
 - [11] C. S. Coates, C. A. Murray, H. L. B. Boström, R. E. M., and A. L. Goodwin, *Mater. Horiz.* **8**, 1446 (2021).
 - [12] T. A. Mary, J. S. O. Evans, T. Vogt, and A. W. Sleight, *Science* **272**, 90 (1996).
 - [13] B. K. Greve, K. L. Martin, P. L. Lee, P. J. Chupas, K. W. Chapman, and A. P. Wilkinson, *J. Am. Chem. Soc.* **132**, 15496 (2010).

- [14] C. S. Coates and A. L. Goodwin, *Mater. Horiz.* **6**, 211 (2019).
- [15] J. W. Zwanziger, *Phys. Rev. B* **76**, 052102 (2007).
- [16] P. Ding, E. J. Liang, Y. Jia, and Z. Y. Du, *J. Phys.: Condens. Matter* **20**, 275224 (2008).
- [17] C. S. Coates, M. Baise, A. Schmutzler, A. Simonov, J. W. Makepeace, A. G. Seel, R. I. Smith, H. Y. Playford, D. A. Keen, R. Siegel, et al., *Nat. Commun.* **12**, 2272 (2021).
- [18] S. T. Bramwell and M. J. Harris, *J. Phys.: Cond. Matt.* **10**, L215 (1998).
- [19] B. C. den Hertog and M. J. P. Gingras, *Phys. Rev. Lett.* **84**, 3430 (2000).
- [20] T. Fennell, P. P. Deen, A. R. Wildes, K. Schamlzl, D. Prabhakaran, A. T. Boothroyd, R. J. Aldus, D. F. McMorrow, and S. T. Bramwell, *Science* **326**, 415 (2009).
- [21] B. Tomasello, C. Castelnovo, R. Moessner, and J. Quintanilla, *Phys. Rev. B* **92**, 155120 (2015).
- [22] C. A. Perottoni and J. A. H. da Jornada, *Science* **280**, 886 (1998).
- [23] J. D. Jorgensen, Z. Hu, S. Teslic, D. N. Argyriou, S. Short, J. S. O. Evans, and A. W. Sleight, *Phys. Rev. B* **59**, 215 (1999).
- [24] K. W. Chapman, G. J. Halder, and P. J. Chupas, *J. Am. Chem. Soc.* **131**, 17546 (2009).
- [25] H. K. Poswal, A. K. Tyagi, A. Lausi, S. K. Deb, and S. M. Sharma, *J. Solid State Chem.* **182**, 136 (2009).
- [26] H. Fang, M. T. Dove, L. H. N. Rimmer, and A. J. Misquitta, *Phys. Rev. B* **88**, 104306 (2013).
- [27] R. Mittal, S. L. Chaplot, and H. Schober, *Appl. Phys. Lett.* **95**, 201901 (2009).
- [28] I. E. Collings, A. B. Cairns, A. L. Thompson, J. E. Parker, C. C. Tang, M. G. Tucker, J. Catafesta, C. Levelut, J. Haines, V. Dmitriev, et al., *J. Am. Chem. Soc.* **135**, 7610 (2013).
- [29] R. A. Secco, J. Liu, N. Imanaka, and G. Adachi, *J. Mater. Sci. Lett.* **20**, 1339 (2001).
- [30] D. A. Keen, A. L. Goodwin, M. G. Tucker, M. T. Dove, J. S. O. Evans, W. A. Crichton, and M. Brunelli, *Phys. Rev. Lett.* **98**, 225501 (2007).
- [31] Y. H. Hu and L. Zhang, *Phys. Rev. B* **81**, 174103 (2010).
- [32] H. Fang and M. T. Dove, *Phys. Rev. B* **87**, 214109 (2013).
- [33] C. S. Coates, J. W. Makepeace, A. G. Seel, M. Baise, B. Slater, and A. L. Goodwin, *Dalton Trans.* **47**, 7263 (2018).
- [34] H. Zhdanov, *C. R. Acad. Sci. URSS* **31**, 352 (1941).
- [35] D. Williams, D. E. Partin, F. J. Lincoln, J. Kouvetakakis, and M. O’Keeffe, *J. Solid State Chem.* **134**, 164 (1997).
- [36] J. L. Manson, W. E. Buschmann, and J. S. Miller, *Angew. Chem. Int. Ed. Engl.* **37**, 783 (1998).
- [37] S. Nishikiori, C. I. Ratcliffe, and J. A. Ripmeester, *J. Chem. Soc., Chem. Commun.* pp. 735–736 (1991).
- [38] S. J. Hibble, A. M. Chippindale, E. Marelli, S. Kroeker, V. K. Michaelis, B. J. Greer, P. M. Aguiar, E. J. Bilb , E. R. Barney, and A. C. Hannon, *J. Am. Chem. Soc.* **135**, 16478 (2013).
- [39] E. Gr neisen, in *Thermische Eigenschaften der Stoffe*, edited by H. Geiger and K. Scheel (Springer, Berlin, 1926), vol. X of *Handbuch der Physik*, pp. 1–59.
- [40] A. L. Goodwin, *Phys. Rev. B* **74**, 134302 (2006).
- [41] U. Werner-Zwanziger, K. W. Chapman, and J. W. Zwanziger, *Z. Phys. Chem.* **226**, 1205 (2012).
- [42] W. F. Kuhs, J. L. Finney, C. Vettier, and D. V. Bliss, *J. Chem. Phys.* **81**, 3612 (1984).
- [43] J. D. Jorgensen, R. A. Beyerlein, N. Watanabe, and T. G. Worlton, *J. Chem. Phys.* **81**, 3211 (1984).
- [44] J.-L. Kuo and M. L. Klein, *J. Phys. Chem. B* **108**, 19634 (2004).
- [45] G. Dehnicke, K. Dehnicke, H. Ahsbahs, and E. Hellner, *Ber. Bunsenges. Phys. Chem.* **78**, 1010 (1974).
- [46] K. W. Chapman and P. J. Chupas, *J. Am. Chem. Soc.* **129**, 10090 (2007).
- [47] T. R. Ravindran, A. K. Arora, S. Chandra, M. C. Valsakumar, and N. V. Chandra Shekar, *Phys. Rev. B* **76**, 054302 (2007).
- [48] R. Mittal, M. Zbiri, H. Schober, E. Marelli, S. J. Hibble, A. M. Chippindale, and S. L. Chaplot, *Phys. Rev. B* **83**, 024301 (2011).
- [49] S. H. Lapidus, G. J. Halder, P. J. Chupas, and K. W. Chapman, *J. Am. Chem. Soc.* **135**, 7621 (2013).
- [50] H. Fang, A. E. Phillips, M. T. Dove, M. G. Tucker, and A. L. Goodwin, *Phys. Rev. B* **88**, 144103 (2013).
- [51] I. Halevy, G. Zamir, M. Winterrose, G. Sanjit, C. R. Grandini, and A. Moreno-Gobbi, *J. Phys.: Conf. Series* **215**, 012013 (2010).
- [52] A. A. Coelho, *TOPAS-Academic, version 4.1 (Computer Software)* (2007).
- [53] P. E. Bl chl, *Phys. Rev. B* **50**, 17953 (1994).
- [54] G. Kresse and J. Hafner, *Phys. Rev. B* **47**, 558 (1993).
- [55] G. Kresse and J. Furthm ller, *Phys. Rev. B* **54**, 11169 (1996).
- [56] G. Kresse and J. Furthm ller, *Comput. Mater. Sci.* **6**, 15 (1996).
- [57] J. P. Perdew, K. Burke, and M. Ernzerhof, *Phys. Rev. Lett.* **77**, 3865 (1996).
- [58] P. Pulay, *Mol. Phys.* **17**, 197 (1969).
- [59] M. Hebbache and M. Zemzemi, *Phys. Rev. B* **70**, 224107 (2004).
- [60] A. Togo and I. Tanaka, *Scr. Mater.* **108**, 1 (2015).
- [61] A. Togo, L. Chaput, I. Tanaka, and G. Hug, *Phys. Rev. B* **81**, 174301 (2010).
- [62] F. Birch, *Phys. Rev.* **71**, 809 (1847).
- [63] N. Sata, G. Shen, M. L. Rivers, and S. R. Sutton, *Phys. Rev. B* **65**, 104114 (2002).
- [64] T. R. Ravindran, A. K. Arora, and T. A. Mary, *Phys. Rev. Lett.* **84**, 3879 (2000).
- [65] B. J. Campbell, H. T. Stokes, D. E. Tanner, and D. M. Hatch, *J. Appl. Cryst.* **39**, 607 (2006).
- [66] J. D. M. Champion, S. T. Bramwell, P. C. W. Holdsworth, and M. J. Harris, *Europhys. Lett.* **57**, 93 (2002).
- [67] M. J. Cliffe, J. A. Hill, C. A. Murray, F.-X. Coudert, and A. L. Goodwin, *Phys. Chem. Chem. Phys.* **17**, 11586 (2015).
- [68] S. Dissegna, P. Vervoorts, C. L. Hobday, T. D ren, D. Daisenberger, A. J. Smith, R. A. Fischer, and G. Kieslich, *J. Am. Chem. Soc.* **140**, 11581 (2018).
- [69] R. M. Lynden-Bell and K. H. Michel, *Rev. Mod. Phys.* **68**, 721 (1994).
- [70] J. M. Bijvoet and J. A. Lely, *Rec. Trav. Chim. Pays-Bas* **59**, 908 (1940).
- [71] D. L. Decker, R. A. Beyerlein, G. Roullet, and T. G. Worlton, *Phys. Rev. B* **10**, 3584 (1974).
- [72] J. M. Rowe, J. J. Rush, and E. Prince, *J. Chem. Phys.* **66**, 5147 (1977).
- [73] W. Dultz and H. Krause, *Phys. Rev. B* **18**, 394 (1978).
- [74] H. T. Stokes, D. L. Decker, H. M. Nelson, and J. D. Jorgensen, *Phys. Rev. B* **47**, 11082 (1993).
- [75] T. Kitazawa, S.-I. Nishikiori, A. Yamagishi, R. Kuroda, and T. Iwamoto, *J. Chem. Soc., Chem. Commun.* pp. 413–415 (1992).
- [76] T. Kitazawa, S.-I. Nishikiori, R. Kuroda, and T. Iwamoto, *J. Chem. Soc., Dalton Trans.* pp. 1029–1036 (1994).
- [77] T. Kitazawa, T. Kikuyama, M. Takahashi, and M. Takeda, *J. Chem. Soc., Dalton Trans.* pp. 2933–2937 (1994).
- [78] T. Kitazawa, S.-I. Nishikiori, and T. Iwamoto, *J. Chem. Soc., Dalton Trans.* pp. 3695–3710 (1994).
- [79] T. Kitazawa, T. Kikuyama, M. Takeda, and T. Iwamoto, *J. Chem. Soc., Dalton Trans.* pp. 3715–3720 (1995).
- [80] T. Iwamoto, *J. Incl. Phen. Mol. Recog. Chem.* **24**, 61 (1996).

- [81] A. E. Phillips, A. L. Goodwin, G. J. Halder, P. D. Southon, and C. J. Kepert, *Angew. Chem. Int. Ed.* **47**, 1396 (2008).